Defect-Engineered Metal−Organic Frameworks: A Thorough Characterization of Active Sites Using CO as a Probe Molecule

Junjun Wang, Weijia Wang, Zhiying Fan, Shuang Chen, Alexei Nefedov, Stefan Heißler, Roland A. Fischer, Christof Wöll,* and Yuemin Wang*

ABSTRACT: Defect engineering (DE) has been recognized as a powerful approach to tune the structural, optical, and chemical properties of metal−organic framework (MOF) materials. Here, a detailed characterization using ultrahigh vacuum Fourier transform infrared spectroscopy and X ray photoelectron spectroscopy was performed for defect engineered NOTT 100 (Cu_2(BPTC), BPTC = biphenyl 3,3′,5,5′ tetracarboxylates). Defects were introduced either via thermal defect engineering (TDE) or the defective linker approach (synthetic defect engineering, SDE). A quantitative analysis of the spectroscopic results revealed the formation of reduced, under coordinated Cu^+/Cu^{2+} dimer defects via both TDE and SDE approaches in a controlled manner. Exposure of the MOFs to CO led to various $(CO)_aCu^+$ and $(CO)_aCu^{2+}$ (a = 1,2) species. The

binding energies of these species as determined by temperature dependent experiments showed strong variations. The type and doping concentration of defective linkers as well as the annealing temperatures played a crucial role in tuning the structural and electronic properties of DE NOTT 100 MOFs. The Brønsted acid sites exposed by protonated carboxylic acids were unambiguously identified by both the characteristic vibrational frequency of adsorbed CO and the corresponding red shift of the acidic OH group.
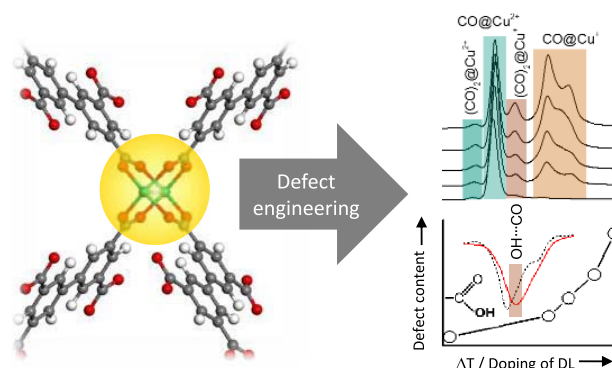
1. INTRODUCTION

Metal−organic frameworks (MOFs) are an emerging class of porous materials that feature unique physical and chemical properties due to the combination of inorganic (nodes) and organic (linkers) building units.[1−6] MOFs exhibit a high degree of crystallinity and large surface areas (up to 10 000 m^2/g).[7] Compared with zeolites, MOFs also possess a higher degree of porosity, and the size of the pores is tunable. These favorable properties, together with the huge number of available frameworks, have led to the introduction of MOFs into a wide range of application fields, including gas storage,[8,9] purification and separation,[10−14] chemical sensing,[15−18] and catalysis.[19,20] Recently, the optical properties of MOFs have also been receiving substantial attention.[21]

MOFs are comprised of diverse metal nodes and organic linkers. After assembly, many MOFs contain coordinatively unsaturated metal sites (CUSs), which show pronounced activity, conferring interesting catalytic properties to numerous MOF materials. The metal cations in MOFs are well defined, isolated, single active metal sites, and can be compared to metal clusters supported on oxides. The application of the latter for heterogeneous catalysis is presently a very active field,[22−28] but the generation and stabilization of metal single sites on oxide substrates remain to be a challenge. Extensive studies have been performed to explore the potential application of MOFs in catalysis,[19,20,29−36] particularly as single site catalysts.[37,38] A variety of intrinsic structural defects in MOFs have been identified.[39−42] Defect engineering (DE) has been recognized as a powerful approach to tailor the chemical properties of MOFs and thus has attracted considerable attention.[43−58]

Cu based DE MOFs with the coexistence of Cu^+ and Cu^{2+} entities have the potential to catalyze various reactions. While structurally perfect HKUST I thin films were observed to be chemically quite inert, the introduction of defects was found to result in high activities for low temperature CO oxidation.[58] In this case, the crystalline nature and precise knowledge of the defect geometry allowed for a thorough analysis of the reaction mechanism, which involves a complex interplay between electronic and steric effects at Cu^+/Cu^{2+} dimers. Here, we present systematic spectroscopic studies on a different type of MOF Cu_2(BPTC) (NOTT 100, BPTC = biphenyl 3,3′,5,5′ tetracarboxylates; see Figure S1), which also contains Cu

dimers. Recent studies have demonstrated that Cu^+ defects can be successfully introduced into this $Cu_2(BPTC)$ framework by incorporating various types of defective linkers.[56] The defect engineered NOTT 100 (DE NOTT 100) was found to show enhanced catalytic activities for the cycloaddition of CO_2 with propylene oxide to propylene carbonate as well as the cyclopropanation of styrene.[56]

In this work, we focus on a fundamental understanding of the structural and electronic properties of various DE NOTT 100 MOFs. By combining temperature dependent ultra high vacuum Fourier transform infrared spectroscopy (UHV FTIRS) and high resolution X ray photoelectron spectroscopy (HR XPS), we are able to provide a detailed characterization of various defects. The IR spectroscopy using CO as a probe molecule has been proven to be a powerful technique to characterize the structural evolution of catalyst surfaces.[59−63] Two different defect engineering strategies were employed to create defects. One is the thermal defect engineering (TDE),[50,57] in which the pristine sample was heated to elevated temperatures under UHV conditions in a controlled manner. The other is synthetic defect engineering (SDE)[47] by doping of NOTT 100 with two defective linkers (Figure S2), biphenyl 3,3′,5 tricarboxylates (L_H) and 5 (5 carboxypyridin 3 yl) isophthalates (L_{Py}). Quantitative analysis based on UHV FTIRS and XPS reveals that the structural and electronic properties of defect sites in DE NOTT 100 can be precisely tailored by both defect engineering approaches. In addition to the modification of metal nodes (Lewis acidic sites) yielding undercoordinated Cu^+/Cu^{2+} dimers, protonated −COOH groups (Brønsted acid sites) are unambiguously identified by the characteristic OH stretching vibration at 3497 cm^{-1} as well as its red shift in frequency induced by CO adsorption via hydrogen bonding.

2. EXPERIMENTAL SECTION

2.1. Synthesis of NOTT-100 Samples.
Pristine NOTT 100 was fabricated using solvothermal synthesis according to the method reported in the literature.[64] The corresponding SDE MOFs Py1 Py3 and H1−H3 were synthesized using analogous procedures by varying the concentration of the incorporated defective linkers L_{Py} and L_H: Py1 (10% L_{Py}), Py2 (30% L_{Py}), Py3 (50% L_{Py}), H1 (19% L_H), H2 (33% L_H), and H3 (59% L_H). The details of the synthesis and characterization (using powder X ray diffraction, ^1H NMR, etc.) are reported elsewhere.[56] The TDE MOFs were obtained via the TDE approach by the temperature induced creation of defects, namely, annealing the pristine NOTT 100 at different temperatures (450, 480, 520, and 550 K) for 30 min under UHV conditions.

2.2. UHV-FTIRS and XPS Measurements.
UHV FTIRS measurements were conducted with a UHV apparatus that combines a state of the art FTIR spectrometer (Bruker Vertex 80v) and a multichamber UHV system (Prevac).[59,65] The samples were first pressed into an inert metal mesh and mounted on a sample holder that was specially designed for the infrared transmission measurements in UHV. The base pressure in the measurement chamber was ∼1 × 10^{-10} mbar. The optical path inside the IR spectrometer and the space between the spectrometer and UHV chamber were also evacuated to avoid atmospheric moisture adsorption and to achieve high sensitivity and stability. The SDE NOTT 100 samples in the UHV chamber were heated to 430 K, aiming to remove the contaminants involved during synthesis and all of

the adsorbed species, e.g., water and hydroxyl groups. Prior to measurement, a spectrum of the clean sample was recorded as a background reference. Carbon monoxide (CO) was used as the probe molecule. The exposure of the sample to CO was carried out by using a leak valve based capillary doser. The infrared data were accumulated by recording 1024 scans with a resolution of 4 cm^{-1}. XPS measurements were carried out in a UHV setup equipped with a high resolution RG Scienta 4000 analyzer.

3. RESULTS AND DISCUSSION

3.1. TDE-NOTT-100: The TDE Approach.
The defect engineered NOTT 100 (DE NOTT 100) MOFs were pre pared by two different strategies: thermal defect engineering (TDE) and synthetic defect engineering (SDE), by incorporat ing various defective linkers into the framework of NOTT 100 during synthesis.

First, we explore the TDE approach,[50,57] i.e., generating defect sites by annealing pristine NOTT 100 at elevated temperatures under UHV conditions. Figure 1a presents the

Figure 1. (a) UHV FTIR difference spectra of CO adsorbed at 100 K on TDE NOTT 100 MOFs prepared by annealing the pristine NOTT 100 at different temperatures for 30 min in UHV. The inset shows the intensity (peak area) ratio of the Cu^+ related bands to the Cu^{2+} related CO bands as a function of the pretreatment temperature. (b) Temperature dependent IR spectra of CO desorption from DE NOTT 100 prepared by the TDE approach at 550 K.

UHV FTIR spectra of CO adsorption at 100 K on NOTT 100 MOFs that were pretreated at different temperatures (from 300 to 550 K) for 30 min under UHV conditions. The pristine NOTT 100 shows just one IR band at 2173 cm^{-1} (Figure 1a), which is attributed to CO species bound to intact Cu^{2+}/Cu^{2+} nodes (CO−Cu^{2+}).[47,58] This finding indicates the formation of nearly defect free NOTT 100, which is further supported by the XPS analysis (∼3% Cu^+).[56] For TDE NOTT 100 MOFs, two low lying vibrations at about 2120 and 2100 cm^{-1} appear and grow on heating the sample to higher temperatures (see Figure 1a). They are characteristic for CO molecules adsorbed to Cu^+ sites (CO−Cu^+),[45,47,58] indicating the creation of reduced Cu^+ CUS using the TDE approach. Furthermore, each Cu site exposed by the Cu^+/Cu^{2+} defect dimers is twofold coordinatively unsaturated and is thus able to bind two CO molecules. Indeed, the corresponding UHV FTIRS data shows two additional IR bands at 2154 and 2195 cm^{-1} (Figure 1a), which are assigned to $(CO)_2$ dimers ligated to Cu^+ and Cu^{2+} CUS, respectively.[47,58] We note that the occurrence of two

Cu^+ related CO bands at 2120 and 2100 cm^{-1} could be due to the presence of various Cu^+ defect sites with slightly different chemical environments.

As shown in Figure 1a, the Cu^+ related CO bands increase in intensity with increasing pretreated temperatures, whereas the Cu^{2+} related peaks gradually attenuate, revealing that the defect concentration increases on annealing the NOTT 100 to higher temperatures. This finding is more clearly presented in the inset of Figure 1a, which plots the ratio of the intensity of Cu^+ to Cu^{2+} related IR bands as a function of preheated temperatures. Overall, our results provide direct evidence that the Cu^+/Cu^{2+} dimer defects can be created via the thermally induced reduction of the pristine Cu^{2+}/Cu^{2+} pairs in a controlled manner.

Temperature dependent UHV FTIR spectroscopy of CO desorption on DE MOFs allows us to gain detailed insight into the binding strength of guest molecules at CUS. As shown in Figure 1b, CO is weakly bound to Cu^{2+} sites with relatively low binding energies. The $(CO)_2-Cu^{2+}$ peak at 2195 cm^{-1} vanishes first at about 130 K, which is followed by the disappearance of the $(CO)-Cu^{2+}$ signal (2174 cm^{-1}) at ~135 K. This reveals the subsequent desorption of the two CO molecules adsorbed at the same Cu^{2+} site. In comparison, the interaction between CO and the Cu^+ defect sites is much stronger, as confirmed by the observation of the desorption of two Cu^+ related CO molecules at higher temperatures: ~145 K for the $(CO)_2-Cu^+$ species at 2154 cm^{-1} and 220−240 K for the $(CO)-Cu^+$ one at frequencies ranging from 2090 to 2140 cm^{-1}. The spectral evolution of the Cu^+ bonded CO vibrations could be related to the modification of the chemical environments along with the desorption of different CO species (see Figure S3). The complex pattern indicates the structural and electronic complexity of the reduced, under coordinated Cu^+/Cu^{2+} dimer defects.

The DE NOTT 100 MOFs prepared by annealing at different temperatures under UHV conditions were further investigated by XPS. Figure 2a displays the deconvoluted Cu 2p XPS data obtained for the pristine NOTT 100 and TDE NOTT 100 MOFs. On the basis of a quantitative analysis, the relative concentration of the Cu^+ species (~933 eV) as a function of the pretreatment temperature is shown in Figure 2b. It can be seen that the content of Cu^+ species increases with increasing heating temperature. These XPS results clearly reveal the creation of Cu^+ defects in the MOF lattice via the controlled thermal reduction of pristine Cu^{2+}/Cu^{2+} dimers at the metal nodes to the Cu^+/Cu^{2+} defects, where both the electronic and structural properties are significantly modified. The XPS observation is in excellent agreement with the UHV FITRS results (see Figure 1a), demonstrating again that thermal defect engineering is an effective approach to introduce defects into the frameworks of NOTT 100.
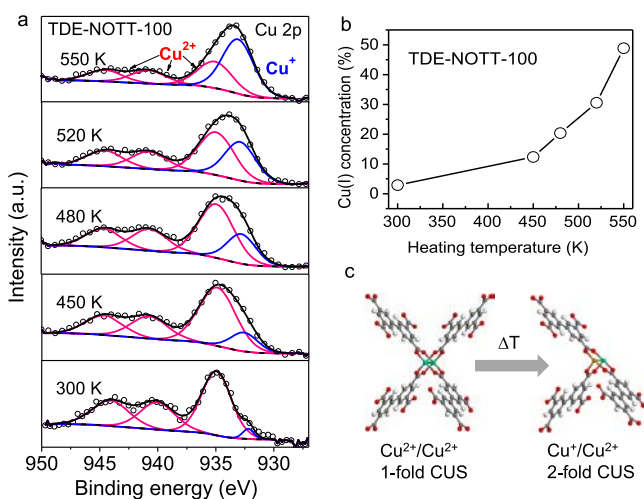
We propose that annealing NOTT 100 to high temperatures leads to Cu^{2+} catalyzed oxidative decarboxylation. Consequently, the Cu^{2+}/Cu^{2+} dimers are partially reduced to Cu^+/Cu^{2+} CUS, as reported for UHM 3[50] and HKUST 1 SURMOFs.[58] In addition, our IR data reveals the appearance and growth of two IR bands at 1707 and 3497 cm^{-1} along with the TDE treatment (see Figure 3). They are ascribed to the
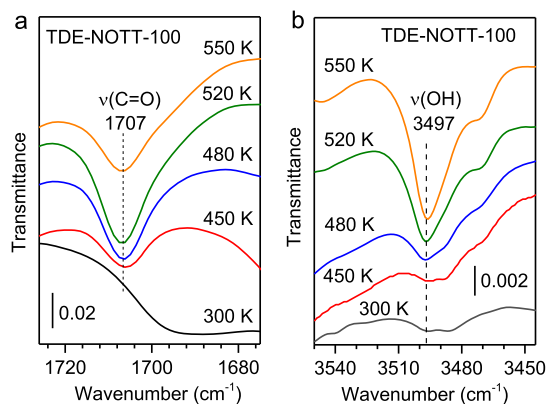
Figure 3. (a) UHV FTIR spectra of the DE NOTT 100 MOFs prepared via the TDE approach by annealing at different temperatures for 30 min under UHV conditions: (a) C=O stretching vibrations and (b) O−H stretching vibrations.

C=O and O−H stretching modes, respectively. Furthermore, the 3497 cm^{-1} band is characteristic of the OH group exposed by carboxylic acids.[66,67] These results indicate that the reduction of Cu^{2+}/Cu^{2+} paddlewheels is also accompanied by the formation of protonated carboxylates exposing free OH groups (Brønsted acid sites). This assignment is further supported by the CO induced frequency shift, as will be discussed later in detail (see Section 3.4).

3.2. SDE-NOTT-100: Doping with Defective Linker L_{Py}.
In addition to the TDE method, it has been reported that DE MOFs can be synthesized via incorporating various defective linkers into the MOF framework.[47,48] Here, a series of SDE NOTT 100 MOFs (Py1 to Py3) were prepared via the SDE approach by doping the pristine NOTT 100 with defective linkers L_{Py1} to L_{Py3}, in which the Cu sites are modified with different concentrations of L_{Py} (5 (5 carboxypyridin 3 yl) isophthalates, Figure S2; for details, see ref 56).

Figure 4 presents the UHV FTIR spectra obtained after CO adsorption at 100 K on different SDE NOTT 100 MOFs. The presence of various Cu related CO species is clearly identified by the characteristic CO bands including $(CO)_2-Cu^{2+}$ at ~2195 cm^{-1}, $CO-Cu^{2+}$ at 2175 cm^{-1}, $(CO)_2-Cu^+$ at 2153 cm^{-1}, and $CO-Cu^+$ centered at ~2106 cm^{-1}, in line with the observation for DE NOTT 100 prepared by the TDE

Figure 2. (a) Deconvoluted XPS data of the TDE NOTT 100 MOFs prepared by annealing at different temperatures for 30 min under UHV conditions. (b) Concentration of Cu^+ species as a function of the pretreatment temperature. (c) Schematic presentation of the creation of DE NOTT 100 MOFs via the TDE approach.
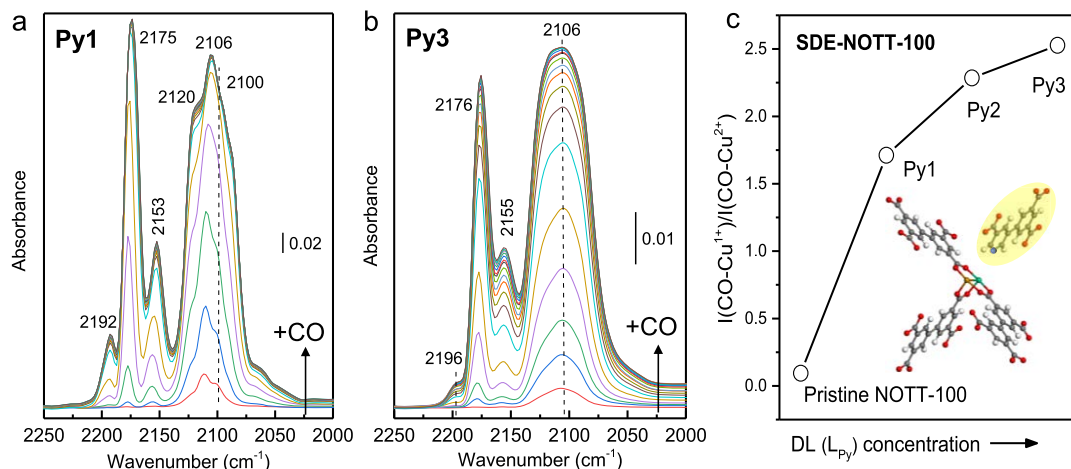
Figure 4. Experimental confirmation of modified copper sites by varying the concentration of the incorporated defective linker L_{Py}. (a, b) UHV FTIR difference spectra obtained after CO adsorption (0.01 mbar for 80 min) at 100 K on SDE NOTT 100 MOFs synthesized by doping with L_{Py}: (a) $[Cu_2(BPTC)_{0.9}(L_{Py})_{0.1}]$ (Py1) and (b) $[Cu_2(BPTC)_{0.5}(L_{Py})_{0.5}]$ (Py3). Prior to exposure, each sample was heated to 430 K to remove all adsorbed species. (c) Integrated intensity ratio of IR bands, i.e., Cu^+ related to Cu^{2+} related, as a function of the defect concentration.
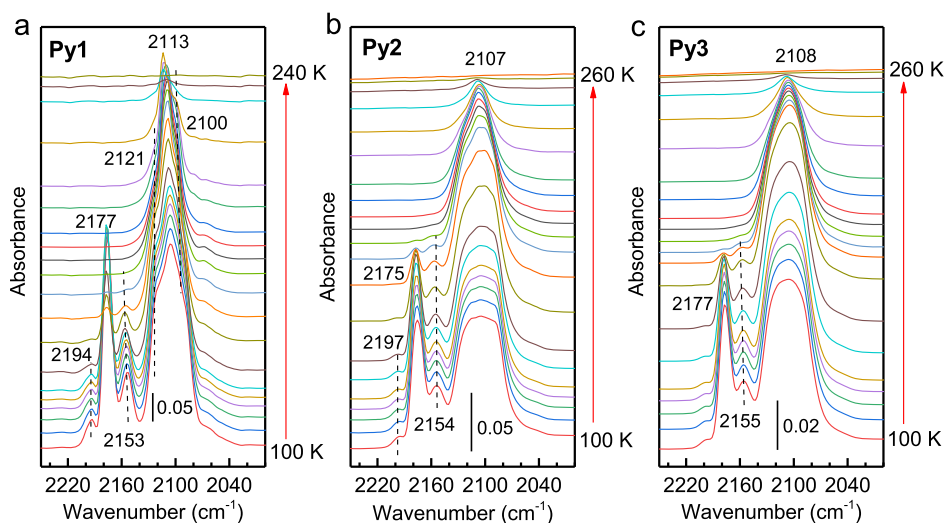
Figure 5. Thermal stability of various CO species adsorbed on SDE MOFs Py1 Py3 monitored by temperature dependent IR spectra. (a−c) UHV FTIR difference spectra obtained after CO adsorption on SDE NOTT 100 MOFs at 100 K and then heating to the indicated temperatures. The SDE MOFs were synthesized by varying the concentration of the incorporated defective linker L_{Py}: (a) $[Cu_2(BPTC)_{0.9}(L_{Py})_{0.1}]$ (Py1), (b) $[Cu_2(BPTC)_{0.7}(L_{Py})_{0.3}]$ (Py2), and (c) $[Cu_2(BPTC)_{0.5}(L_{Py})_{0.5}]$ (Py3).

approach (see Figure 1a). In contrast to pristine NOTT 100, SDE NOTT 100 MOFs are dominated by the intense Cu^+− CO bands, revealing the formation of reduced Cu^+/Cu^{2+} paddlewheel defects after doping of the framework with L_{Py}. Figure 4c shows the integrated intensity ratio of Cu^+ related bands to the CO−Cu^{2+} bands as a function of the defect concentration. The relative intensity of CO−Cu^+ bands significantly increases with increasing content of the L_{Py} linker. These IR results demonstrate the successful incorporation of defective linker L_{Py}, yielding Cu^+/Cu^{2+} defect dimers in a controlled manner.

The thermal stability of various CO species bound to SDE NOTT 100 prepared by doping with defective linker L_{Py} was investigated by temperature dependent UHV FTIRS. Figure 5 shows the IR spectra recorded after exposing SDE NOTT 100 (Py1 to Py3) to CO at 100 K and subsequently heating to higher temperatures. For all samples, the CO bands originating from $(CO)_2$−Cu^{2+}, CO−Cu^{2+}, and $(CO)_2$−Cu^+ disappear at relatively low temperatures up to approximately 150 K,

indicating a low binding energy of CO bound to these Cu sites, whereas the CO−Cu^+ related bands at 2120−2100 cm^{-1} are more stable and disappear only upon heating to 220−240 K, revealing a stronger binding of CO to the reduced Cu^+ CUS because of the enhanced π back donation. These results are in good agreement with the observation for TDE NOTT 100 MOFs as discussed above (see Figure 1b).

3.3. SDE-NOTT-100: Doping with Defective Linker L_H. To gain insight into the influence of different kinds of defective linkers on DE MOFs, a series of SDE NOTT 100 MOFs (H1 to H3) were prepared by introducing defective linkers, L_H (biphenyl 3,3′,5 tricarboxylates, Figure S2; for details, see ref 56). The corresponding UHV FTIRS data were obtained after exposure of the MOF to CO at 100 K (Figure 6). A large number of IR bands are observed, which are attributed to the presence of various Cu^{2+} and Cu^+ related CO species, in line with the results for DE NOTT 100 MOFs prepared by the TDE approach (Figure 1) and by doping with defective linker L_{Py} (Figure 4). Figure 6c shows the integrated intensity ratio of
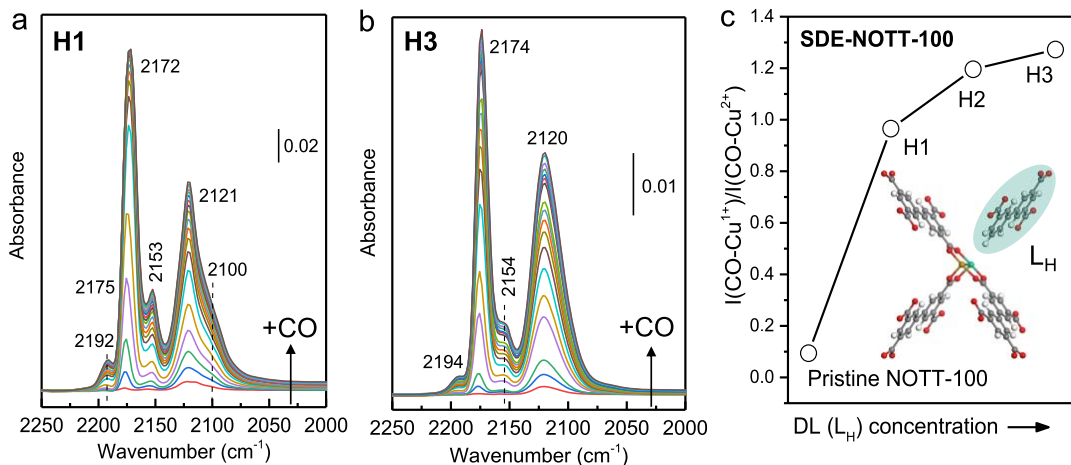
Figure 6. Experimental confirmation of modified copper sites by varying the concentration of the incorporated defective linker L_H. (a, b) UHV FTIR difference spectra obtained after CO adsorption (0.01 mbar for 80 min) at 100 K on SDE NOTT 100 MOFs prepared by doping with L_H: (a) $[Cu_2(BPTC)_{0.81}(L_H)_{0.19}]$ (H1) and (b) $[Cu_2(BPTC)_{0.41}(L_H)_{0.59}]$ (H3). Prior to exposure, each sample was heated to 430 K to remove all adsorbed species. (c) Integrated intensity ratio of IR bands, i.e., Cu^+ related to Cu^{2+} related, as a function of the defect concentration.
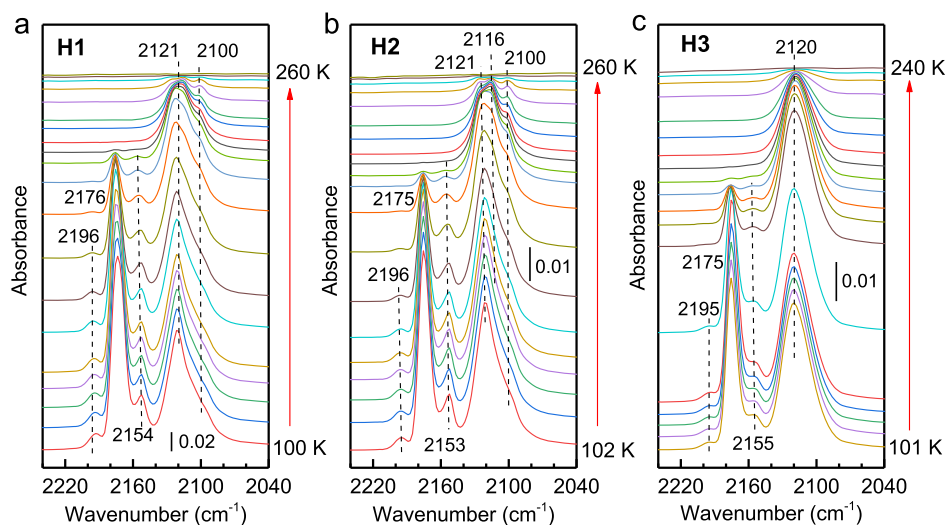
Figure 7. Thermal stability of various CO species adsorbed on H1−H3 monitored by temperature dependent IR spectra. (a−c) UHV FTIR difference spectra obtained after CO adsorption on SDE NOTT 100 MOFs (H1−H3) at ∼100 K and then heating to the indicated temperatures. The SDE MOFs were synthesized by varying the concentration of the incorporated defective linker L_H: (a) $[Cu_2(BPTC)_{0.81}(L_H)_{0.19}]$ (H1), (b) $[Cu_2(BPTC)_{0.67}(L_H)_{0.33}]$ (H2), and (c) $[Cu_2(BPTC)_{0.41}(L_H)_{0.59}]$ (H3).

the CO−Cu^+ bands to the CO−Cu^{2+} ones for different SDE NOTT 100 MOFs (H1−H3). The fraction of the Cu^+ defects clearly increases with increasing defect concentration, revealing a controlled creation of electron enriched Cu^+/Cu^{2+} defects.

Interestingly, for Py1 (Figure 4a) and H1 (Figure 6a), the Cu^+ bonded CO vibrations are characterized by a more complex spectra pattern, whereas only one broad CO−Cu^+ band between 2140 and 2090 cm^{-1} appears for Py3 (Figure 4b) and H3 (Figure 6b). This finding reveals that the superimposed bands cannot be resolved in Py3 and H3, which is probably due to the increased complexity in both electronic and steric properties with increasing concentration of defective linkers L_{Py} and L_H.

The corresponding temperature dependent UHV FTIRS results are displayed in Figure 7. These IR data provide detailed information about the thermal stability of various $(CO)_a$−Cu^+ and $(CO)_a$−Cu^{2+} (a = 1 or 2) species, which is in excellent agreement with the observation for DE NOTT 100 MOFs prepared using other DE approaches (see Figures 1b

and 5). Overall, close inspections of the UHV FTIRS results show that the spectral evolution depends strongly on the doping type and level of defect linkers, which lead to the formation of various Cu related CO species with different binding energies.

The comprehensive IR results show that the framework incorporation of both defective linkers L_{Py} and L_H into pristine NOTT 100 leads to a significant increase of the relative intensity of the CO−Cu^+ bands, confirming the generation of type I defects (modified metal paddlewheels). However, a close analysis of the IR data for DE NOTT 100 MOFs, prepared by incorporating with L_{Py} and L_H in comparable doping levels, reveals that the relative intensity (peak area) of CO−Cu^+ bands of H1 and H3 (Figure 6a,b) is much lower than that of Py1 and Py3 (Figure 4a,b), although a comparable doping concentration of L_{Py} and L_H was adopted. These findings imply that the L_H incorporation prefers to generate type II defects (i.e., missing metal paddlewheels). However, in the case of defective linker L_{Py}, the pyridyl N atom acts as a
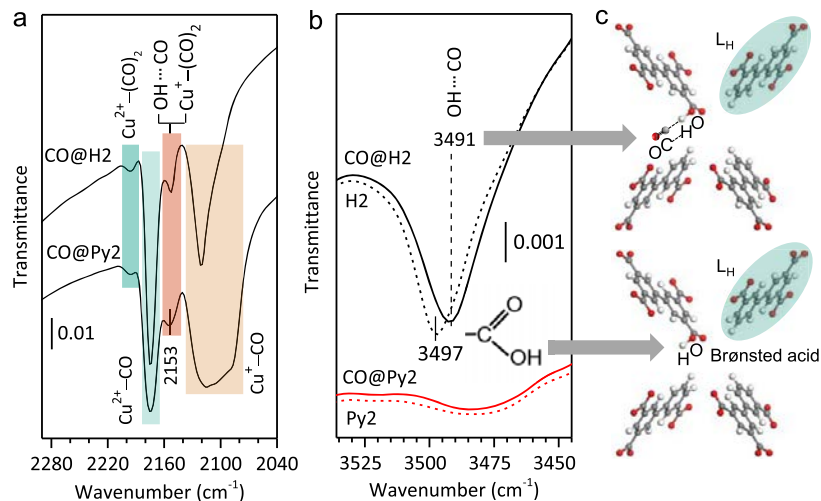
Figure 8. UHV FTIR spectra recorded after CO adsorption (0.01 mbar) at 100 K on $[Cu_2(BPTC)_{0.67}(L_H)_{0.33}]$ (H2) and $[Cu_2(BPTC)_{0.7}(L_{Py})_{0.3}]$ (Py2): (a) CO vibrations and (b) OH vibrations. For comparison, the spectra in the OH region obtained before CO adsorption are shown as dashed lines. (c) Brønsted acid sites (OH) exposed by carboxylic acids at metal node vacancies, which are generated via incorporating defective linker L_H. Lower panel: "free" COOH; upper panel: CO adsorption on OH via H bonding.
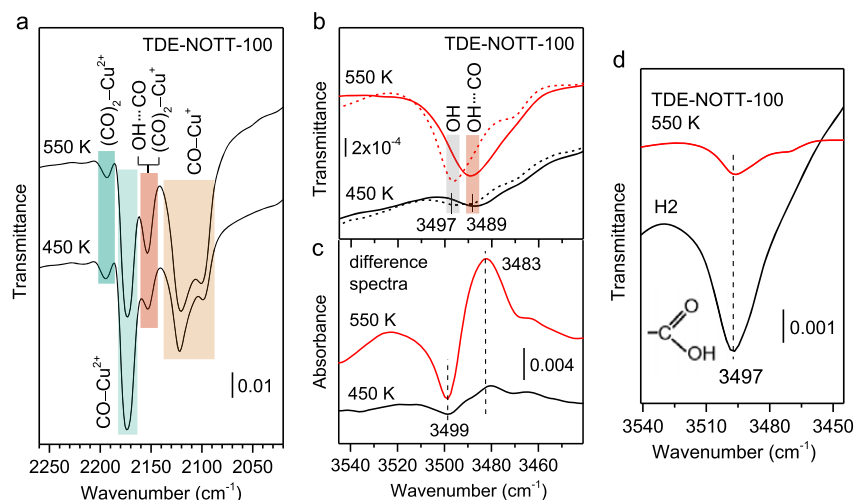
Figure 9. (a, b) UHV FTIR spectra recorded after CO adsorption (0.01 mbar) at 100 K on DE NOTT 100 MOFs prepared via the TDE approach by annealing at different temperatures for 30 min under UHV conditions: (a) CO vibrations and (b) OH vibrations (the spectra obtained before CO adsorption are shown as dashed lines). (c) Corresponding difference spectra recorded after CO adsorption at 100 K on DE NOTT 100 MOFs. (d) Comparison of the UHV FTIR spectra of DE NOTT 100 MOFs prepared via different approaches: TDE NOTT 100 and H2 (SDE NOTT 100).

Lewis base ligand that weakly interacts with Cu cations (Lewis acid sites). We propose that the creation of metal node vacancies is suppressed by this metal−ligand interaction.[56]

3.4. Brønsted Acid Sites in DE-NOTT-100 MOFs. The present results demonstrate that the structural and electronic properties of NOTT 100 can be substantially modified by the TDE approach or incorporation of defect linkers (i.e., the SDE method), which consequently has a significant impact on their chemical reactivity.[56] As discussed above, our IR data show that the type II defects are the dominant ones generated in DE NOTT 100 MOFs of H1−H3. This will facilitate the formation of Brønsted acid sites originating from protonated carboxylates with dangling OH groups. In contrast, for DE NOTT 100 MOFs of Py1 to Py3, the type I defects are the major ones that expose Lewis acid sites at the metal CUS.

IR spectroscopy is also capable of identifying the Brønsted acid site. Pyridine is usually used as the probe molecule to determine the density of Brønsted acid sites. However, it is not well suited for the detection of Brønsted acid sites in MOFs, because its vibrations overlap with the vibrations of the MOF framework.[68] In this work, CO was successfully used as a probe molecule to monitor Brønsted acid sites formed in DE NOTT 100. It is known that the binding of CO to acidic OH sites will result in a shift of the OH stretching vibration to lower frequencies.[69] Thus, CO is suitable for detecting the Brønsted acid sites in MOFs.[70]

Figure 8 shows the UHV FTIR spectra in the regions of CO (Figure 8a) and OH (Figure 8b) vibrations obtained before and after CO adsorption at 100 K on two representative DE NOTT 100 MOFs: H2 and Py2. The two DE MOF samples contain defective linkers (L_H/L_{Py}) with comparable concentrations ($\sim$30%). For the DE MOF H2, we clearly observe an OH stretching band at 3497 cm^{-1} that is characteristic of hydroxyl groups of protonated carboxylates (Figure 8c).[66,67]

Exposing H2 to CO leads to a slight shift of the OH vibration to 3491 cm^{-1}. This CO induced frequency shift is attributed to the weak interaction between CO and hydroxyls via hydrogen bonding (Figure 8c). Interestingly, the IR data for DE MOF Py2 does not show any indications for the presence of such "free" or CO adsorbed OH groups (Figure 8b). According to the literature,[68−70] the OH related CO vibration is located at about 2155 cm^{-1}, which is overlapped with the $(CO)_2-Cu^+$ species. However, a close look at the IR data reveals that for H2, the intensity (peak area) ratio between the 2153 cm^{-1} band and the $CO-Cu^+$ bands is higher than that of Py2 (Figure 8a). Considering the fact that much fewer Cu^+ defects are formed in H2 compared with Py2, the more intense signal at 2153 cm^{-1} is attributed to the presence of OH bonded CO species in H2.

These IR results provide direct evidence that the doping of NOTT 100 with L_H, instead of L_{Py}, promotes the generation of protonated carboxylates exposing Brønsted acid sites in DE NOTT 100. As shown in Figure 8c, the acidic OH groups exposed by carboxylic acids are formed along with the creation of metal node vacancies. We note that despite the importance of protonated carboxylic acids as functional groups in MOFs, a thorough characterization using IR spectroscopy has not been achieved so far.

The Brønsted acid sites are also identified by IR using CO as a probe molecule (Figure 9a) for DE NOTT 100 MOFs, prepared via the TDE method by annealing NOTT 100 at different temperatures. A shown in Figure 9b, the corresponding IR spectra reveal a typical OH band at 3497 cm^{-1}, which shifts to a lower frequency (3489 cm^{-1}) due to the weak interaction with CO. The latter is further characterized by the OH bonded CO vibration at 2154 cm^{-1} (Figure 9a), in line with the observation for H2 (Figure 8a). However, the OH signal observed for TDE NOTT 100 samples is about an order of magnitude weaker in intensity than that of H2 (see Figure 9d), revealing that protonated carboxylic acids exist only as minority species in DE NOTT 100 prepared via the TDE method. Since the oxidative decarboxylation does not yield COOH groups, we speculate that this small density of free acid groups is attributed to the rupture of carboxylate−$(Cu^{2+})_2$ bonds, caused by mechanical stress resulting from the thermally induced creation of defects.

In comparison to SDE, the TDE approach enables to create more undercoordinated single active sites by removing guest molecules bound to metal nodes via annealing at elevated temperatures. More importantly, TDE allows to precisely tune the electronic and steric properties of metal nodes via the controlled thermal reduction of pristine Cu^{2+}/Cu^{2+} dimers while retaining the structural integrity of the framework. This feature makes TDE an efficient method, in particular, for the generation of defects in mixed metal MOFs (e.g., CuPd HKUST 1[53] and RuRh HKUST 1 MOFs[57]).

4. CONCLUSIONS

In this work, the local chemical environments of Cu paddlewheel nodes in the defect engineered NOTT 100 MOFs were characterized using temperature resolved UHV FTIRS in conjunction with HR XPS. The DE NOTT 100 MOFs were prepared using two different defect engineering strategies: thermal defect engineering (TDE) and synthetic defect engineering (SDE) by doping with defective linkers. The combined results demonstrate that the structural and electronic properties of DE NOTT 100 MOFs can be modified by both approaches in a controlled manner. The temperature dependent UHV FTIRS provides detailed insight into the thermal stability of various $(CO)_a-Cu^+$ and $(CO)_a-Cu^{2+}$ (a = 1 or 2) species. The observation of geminal $(CO)_2$ dimers on Cu^+ and Cu^{2+} CUS reveals the steric modification on both defect sites that are twofold coordinatively unsaturated. Importantly, the interplay between steric and electronic effects at reduced Cu^+/Cu^{2+} defect nodes allows for tailoring the chemical reactivity of Cu MOFs as single site catalysts.[58]

Furthermore, the comprehensive IR results reveal that the incorporation of defective linker L_H preferentially forms type II defects (metal node vacancies), whereas the type I defects (modified metal paddlewheels) are identified as the predominant ones in Py Py3. Type II defects in H1−H3 facilitate the generation of protonated carboxylic acids exposing free OH groups as Brønsted acid sites in DE MOFs. The latter were unambiguously identified by the characteristic stretching mode at 3497 cm^{-1} and its red shift induced by the weak interaction with CO via hydrogen bonding. In addition, our IR data provided evidence for the presence of Brønsted acid sites inside DE NOTT 100 prepared via the TDE approach, in which the protonated carboxylate groups are formed along with the partial thermal reduction of pristine Cu^{2+}/Cu^{2+} dimers.

AUTHOR INFORMATION

Corresponding Authors

Christof Wöll − *Institute of Functional Interfaces (IFG), Karlsruhe Institute of Technology (KIT), 76344 Eggenstein Leopoldshafen, Germany*; Email: christof.woell@kit.edu

Yuemin Wang − *Institute of Functional Interfaces (IFG), Karlsruhe Institute of Technology (KIT), 76344 Eggenstein Leopoldshafen, Germany*; ⊙ orcid.org/0000 0002 9963 5473; Email: yuemin.wang@kit.edu

Authors

Junjun Wang − *Institute of Functional Interfaces (IFG), Karlsruhe Institute of Technology (KIT), 76344 Eggenstein Leopoldshafen, Germany*

Weijia Wang − *Institute of Functional Interfaces (IFG), Karlsruhe Institute of Technology (KIT), 76344 Eggenstein Leopoldshafen, Germany*

Zhiying Fan − *Catalysis Research Center and Faculty of Chemistry, Technical University of Munich, D 85747 Garching, Germany*

Shuang Chen − *Institute of Functional Interfaces (IFG), Karlsruhe Institute of Technology (KIT), 76344 Eggenstein Leopoldshafen, Germany*

Alexei Nefedov − *Institute of Functional Interfaces (IFG), Karlsruhe Institute of Technology (KIT), 76344 Eggenstein Leopoldshafen, Germany*; ⊙ orcid.org/0000 0003 2771 6386

Stefan Heißler − *Institute of Functional Interfaces (IFG), Karlsruhe Institute of Technology (KIT), 76344 Eggenstein Leopoldshafen, Germany*

Roland A. Fischer − *Catalysis Research Center and Faculty of Chemistry, Technical University of Munich, D 85747 Garching, Germany;* ⓞ orcid.org/0000 0002 7532 5286

Notes

The authors declare no competing financial interest.

REFERENCES

(1) Kitagawa, S.; Kitaura, R.; Noro, S. Functional Porous Coordination Polymers. *Angew. Chem., Int. Ed.* **2004**, *43*, 2334−2375.

(2) Férey, G. Hybrid Porous Solids: Past, Present, Future. *Chem. Soc. Rev.* **2008**, *37*, 191−214.

(3) Rowsell, J. L. C.; Yaghi, O. M. Metal Organic Frameworks: A New Class of Porous Materials. *Microporous Mesoporous Mater.* **2004**, *73*, 3−14.

(4) Long, J. R.; Yaghi, O. M. The Pervasive Chemistry of Metal Organic Frameworks. *Chem. Soc. Rev.* **2009**, *38*, 1213−1214.

(5) Zacher, D.; Shekhah, O.; Wöll, C.; Fischer, R. A. Thin Films of Metal Organic Frameworks. *Chem. Soc. Rev.* **2009**, *38*, 1418−1429.

(6) Liu, J. X.; Wöll, C. Surface Supported Metal Organic Framework Thin Films: Fabrication Methods, Applications, and Challenges. *Chem. Soc. Rev.* **2017**, *46*, 5730−5770.

(7) Furukawa, H.; Cordova, K. E.; O'Keeffe, M.; Yaghi, O. M. The Chemistry and Applications of Metal Organic Frameworks. *Science* **2013**, *341*, No. 1230444.

(8) Murray, L. J.; Dinca, M.; Long, J. R. Hydrogen Storage in Metal Organic Frameworks. *Chem. Soc. Rev.* **2009**, *38*, 1294−1314.

(9) Farha, O. K.; Yazaydın, A. Ö.; Eryazici, I.; Malliakas, C. D.; Hauser, B. G.; Kanatzidis, M. G.; Nguyen, S. T.; Snurr, R. Q.; Hupp, J. T. De Novo Synthesis of a Metal−Organic Framework Material Featuring Ultrahigh Surface Area and Gas Storage Capacities. *Nat. Chem.* **2010**, *2*, 944−948.

(10) Schröder, M. *Functional Metal Organic Frameworks: Gas Storage, Separation and Catalysis*; Springer: 2010; Vol. 293.

(11) Bloch, E. D.; Queen, W. L.; Krishna, R.; Zadrozny, J. M.; Brown, C. M.; Long, J. R. Hydrocarbon Separations in a Metal Organic Framework with Open Iron(II) Coordination Sites. *Science* **2012**, *335*, 1606−1610.

(12) Chen, B. L.; Liang, C. D.; Yang, J.; Contreras, D. S.; Clancy, Y. L.; Lobkovsky, E. B.; Yaghi, O. M.; Dai, S. A Microporous Metal Organic Framework for Gas Chromatographic Separation of Alkanes. *Angew. Chem., Int. Ed.* **2006**, *45*, 1390−1393.

(13) Li, X.; Liu, Y. X.; Wang, J.; Gascon, J.; Li, J. S.; Van der Bruggen, B. Metal Organic Frameworks Based Membranes for Liquid Separation. *Chem. Soc. Rev.* **2017**, *46*, 7124−7144.

(14) Li, J. R.; Sculley, J.; Zhou, H. C. Metal Organic Frameworks for Separations. *Chem. Rev.* **2012**, *112*, 869−932.

(15) Hu, Z.; Deibert, B. J.; Li, J. Luminescent Metal−Organic Frameworks for Chemical Sensing and Explosive Detection. *Chem. Soc. Rev.* **2014**, *43*, 5815−5840.

(16) Zhang, M.; Feng, G.; Song, Z.; Zhou, Y. P.; Chao, H. Y.; Yuan, D.; Tan, T. T.; Guo, Z.; Hu, Z.; Tang, B. Z.; et al. Two Dimensional Metal−Organic Framework with Wide Channels and Responsive Turn on Fluorescence for the Chemical Sensing of Volatile Organic Compounds. *J. Am. Chem. Soc.* **2014**, *136*, 7241−7244.

(17) Kreno, L. E.; Leong, K.; Farha, O. K.; Allendorf, M.; Van Duyne, R. P.; Hupp, J. T. Metal Organic Framework Materials as Chemical Sensors. *Chem. Rev.* **2012**, *112*, 1105−1125.

(18) Stassen, I.; Burtch, N. C.; Talin, A. A.; Falcaro, P.; Allendorf, M. D.; Ameloot, R. An Updated Roadmap for the Integration of Metal Organic Frameworks with Electronic Devices and Chemical Sensors. *Chem. Soc. Rev.* **2017**, *46*, 3185−3241.

(19) Farrusseng, D.; Aguado, S.; Pinel, C. Metal−Organic Frameworks: Opportunities for Catalysis. *Angew. Chem., Int. Ed.* **2009**, *48*, 7502−7513.

(20) Corma, A.; García, H.; Llabrés i Xamena, F. X. Engineering Metal Organic Frameworks for Heterogeneous Catalysis. *Chem. Rev.* **2010**, *110*, 4606−4655.

(21) Haldar, R.; Heinke, L.; Wöll, C. Advanced Photoresponsive Materials Using the Metal−Organic Framework Approach. *Adv. Mater.* **2020**, *32*, No. 1905227.

(22) Maurer, F.; Jelic, J.; Wang, J.; Gänzler, A.; Dolcet, P.; Wöll, C.; Wang, Y.; Studt, F.; Casapu, M.; Grunwaldt, J. D. Tracking the Formation, Fate and Consequence for Catalytic Activity of Pt Single Sites on CeO2. *Nat. Catal.* **2020**, *3*, 824−833.

(23) Qiao, B.; Wang, A.; Yang, X.; Allard, L. F.; Jiang, Z.; Cui, Y.; Liu, J.; Li, J.; Zhang, T. Single Atom Catalysis of CO Oxidation Using Pt1/FeOx. *Nat. Chem.* **2011**, *3*, 634−641.

(24) Cargnello, M.; Doan Nguyen, V. V. T.; Gordon, T. R.; Diaz, R. E.; Stach, E. A.; Gorte, R. J.; Fornasiero, P.; Murray, C. B. Control of Metal Nanocrystal Size Reveals Metal Support Interface Role for Ceria Catalysts. *Science* **2013**, *341*, 771−773.

(25) Herzing, A. A.; Kiely, C. J.; Carley, A. F.; Landon, P.; Hutchings, G. J. Identification of Active Gold Nanoclusters on Iron Oxide Supports for CO Oxidation. *Science* **2008**, *321*, 1331−1335.

(26) Dvořák, F.; Camellone, M. F.; Tovt, A.; Tran, N. D.; Negreiros, F. R.; Vorokhta, M.; Ska'la, T.; Matolínova', I.; Mysliveček, J.; Matolín, V.; et al. Creating Single Atom Pt Ceria Catalysts by Surface Step Decoration. *Nat. Commun.* **2016**, *7*, No. 10801.

(27) Therrien, A. J.; Hensley, A. J. R.; Marcinkowski, M. D.; Zhang, R.; Lucci, F. R.; Coughlin, B.; Schilling, A. C.; McEwen, J. S.; Sykes, E. C. H. An Atomic Scale View of Single Site Pt Catalysis for Low Temperature CO Oxidation. *Nat. Catal.* **2018**, *1*, 192−198.

(28) Ye, C.; Zhang, N.; Wang, D.; Li, Y. Single Atomic Site Catalysts: Synthesis, Characterization, and Applications. *Chem. Commun.* **2020**, *56*, 7687−7697.

(29) Lee, J.; Farha, O. K.; Roberts, J.; Scheidt, K. A.; Nguyen, S. T.; Hupp, J. T. Metal Organic Framework Materials as Catalysts. *Chem. Soc. Rev.* **2009**, *38*, 1450−1459.

(30) Yoon, M.; Srirambalaji, R.; Kim, K. Homochiral Metal Organic Frameworks for Asymmetric Heterogeneous Catalysis. *Chem. Rev.* **2012**, *112*, 1196−1231.

(31) Noei, H.; Amirjalayer, S.; Muller, M.; Zhang, X. N.; Schmid, R.; Muhler, M.; Fischer, R. A.; Wang, Y. Low Temperature CO Oxidation over Cu Based Metal Organic Frameworks Monitored by Using FTIR Spectroscopy. *ChemCatChem* **2012**, *4*, 755−759.

(32) Valvekens, P.; Vermoortele, F.; De Vos, D. Metal Organic Frameworks as Catalysts: The Role of Metal Active Sites. *Catal. Sci. Technol.* **2013**, *3*, 1435−1445.

(33) Dhakshinamoorthy, A.; Garcia, H. Metal Organic Frameworks as Solid Catalysts for the Synthesis of Nitrogen Containing Hetero cycles. *Chem. Soc. Rev.* **2014**, *43*, 5750−5765.

(34) Liu, J.; Chen, L.; Cui, H.; Zhang, J.; Zhang, L.; Su, C. Y. Applications of Metal−Organic Frameworks in Heterogeneous Supramolecular Catalysis. *Chem. Soc. Rev.* **2014**, *43*, 6011−6061.

(35) Zhu, L.; Liu, X. Q.; Jiang, H. L.; Sun, L. B. Metal Organic Frameworks for Heterogeneous Basic Catalysis. *Chem. Rev.* **2017**, *117*, 8129−8176.

(36) Huang, Y. B.; Liang, J.; Wang, X. S.; Cao, R. Multifunctional Metal Organic Framework Catalysts: Synergistic Catalysis and Tandem Reactions. *Chem. Soc. Rev.* **2017**, *46*, 126−157.

(37) Rogge, S. M.; Bavykina, A.; Hajek, J.; Garcia, H.; Olivos Suarez, A. I.; Sepúlveda Escribano, A.; Vimont, A.; Clet, G.; Bazin, P.; Kapteijn, F.; et al. Metal−Organic and Covalent Organic Frameworks as Single Site Catalysts. *Chem. Soc. Rev.* **2017**, *46*, 3134−3184.

(38) Wang, Y.; Wöll, C. Chemical Reactions at Isolated Single Sites inside Metal Organic Frameworks. *Catal. Lett.* **2018**, *148*, 2201−2222.

(39) Shôâeè, M.; Agger, J. R.; Anderson, M. W.; Attfield, M. P. Crystal Form, Defects and Growth of the Metal Organic Framework HKUST 1 Revealed by Atomic Force Microscopy. *CrystEngComm* **2008**, *10*, 646−648.

(40) Ameloot, R.; Vermoortele, F.; Hofkens, J.; De Schryver, F. C.; De Vos, D. E.; Roeffaers, M. B. Three Dimensional Visualization of Defects Formed During the Synthesis of Metal−Organic Frameworks: A Fluorescence Microscopy Study. *Angew. Chem., Int. Ed.* **2013**, *52*, 401−405.

(41) Fang, Z.; Bueken, B.; De Vos, D. E.; Fischer, R. A. Defect Engineered Metal−Organic Frameworks. *Angew. Chem., Int. Ed.* **2015**, *54*, 7234−7254.

(42) Liu, L.; Chen, Z.; Wang, J.; Zhang, D.; Zhu, Y.; Ling, S.; Huang, K. W.; Belmabkhout, Y.; Adil, K.; Zhang, Y.; et al. Imaging Defects and Their Evolution in a Metal−Organic Framework at Sub Unit Cell Resolution. *Nat. Chem.* **2019**, *11*, 622−628.

(43) Ravon, U.; Savonnet, M.; Aguado, S.; Domine, M. E.; Janneau, E.; Farrusseng, D. Engineering of Coordination Polymers for Shape Selective Alkylation of Large Aromatics and the Role of Defects. *Microporous Mesoporous Mater.* **2010**, *129*, 319−329.

(44) Marx, S.; Kleist, W.; Baiker, A. Synthesis, Structural Properties, and Catalytic Behavior of Cu BTC and Mixed Linker Cu BTC PyDC in the Oxidation of Benzene Derivatives. *J. Catal.* **2011**, *281*, 76−87.

(45) St Petkov, P.; Vayssilov, G. N.; Liu, J. X.; Shekhah, O.; Wang, Y.; Wöll, C.; Heine, T. Defects in MOFs: A Thorough Character ization. *ChemPhysChem* **2012**, *13*, 2025−2029.

(46) Wu, H.; Chua, Y. S.; Krungleviciute, V.; Tyagi, M.; Chen, P.; Yildirim, T.; Zhou, W. Unusual and Highly Tunable Missing Linker Defects in Zirconium Metal Organic Framework UiO 66 and Their Important Effects on Gas Adsorption. *J. Am. Chem. Soc.* **2013**, *135*, 10525−10532.

(47) Fang, Z. L.; Dürholt, J. P.; Kauer, M.; Zhang, W.; Lochenie, C.; Jee, B.; Albada, B.; Metzler Nolte, N.; Pöppl, A.; Weber, B.; et al. Structural Complexity in Metal Organic Frameworks: Simultaneous Modification of Open Metal Sites and Hierarchical Porosity by Systematic Doping with Defective Linkers. *J. Am. Chem. Soc.* **2014**, *136*, 9627−9636.

(48) Kozachuk, O.; Luz, I.; Llabrés i Xamena, F. X.; Noei, H.; Kauer, M.; Albada, H. B.; Bloch, E. D.; Marler, B.; Wang, Y.; Muhler, M. F.; et al. Multifunctional, Defect Engineered Metal Organic Frameworks with Ruthenium Centers: Sorption and Catalytic Properties. *Angew. Chem., Int. Ed.* **2014**, *53*, 7058−7062.

(49) Trickett, C. A.; Gagnon, K. J.; Lee, S.; Gandara, F.; Burgi, H. B.; Yaghi, O. M. Definitive Molecular Level Characterization of Defects in UiO 66 Crystals. *Angew. Chem., Int. Ed.* **2015**, *54*, 11162−11167.

(50) Wang, Z. B.; Sezen, H.; Liu, J.; Yang, C.; Roggenbuck, S. E.; Peikert, K.; Fröba, M.; Mavrandonakis, A.; Supronowicz, B.; Heine, T.; et al. Tunable Coordinative Defects in UHM 3 Surface Mounted MOFs for Gas Adsorption and Separation: A Combined Experimental and Theoretical Study. *Microporous Mesoporous Mater.* **2015**, *207*, 53−60.

(51) Liu, Y. Y.; Klet, R. C.; Hupp, J. T.; Farha, O. Probing the Correlations between the Defects in Metal Organic Frameworks and Their Catalytic Activity by an Epoxide Ring Opening Reaction. *Chem. Commun.* **2016**, *52*, 7806−7809.

(52) Zhang, W. H.; Kauer, M.; Halbherr, O.; Epp, K.; Guo, P.; Gonzalez, M. I.; Xiao, D. J.; Wiktor, C.; Llabrés i Xamena, F. X.; Wöll, C.; et al. Ruthenium Metal Organic Frameworks with Different Defect Types: Influence on Porosity, Sorption, and Catalytic Properties. *Chem. − Eur. J.* **2016**, *22*, 14297−14307.

(53) Guo, P. H.; Froese, C.; Fu, Q.; Chen, Y. T.; Peng, B. X.; Kleist, W.; Fischer, R. A.; Muhler, M.; Wang, Y. CuPd Mixed Metal HKUST 1 as a Catalyst for Aerobic Alcohol Oxidation. *J. Phys. Chem. C* **2018**, *122*, 21433−21440.

(54) Dissegna, S.; Epp, K.; Heinz, W. R.; Kieslich, G.; Fischer, R. A. Defective Metal Organic Frameworks. *Adv. Mater.* **2018**, *30*, No. 1704501.

(55) Guo, P. H.; Fu, Q.; Yildiz, C.; Chen, Y. T.; Ollegott, K.; Froese, C.; Kleist, W.; Fischer, R. A.; Wang, Y.; Muhler, M.; et al. Regulating the Size and Spatial Distribution of Pd Nanoparticles Supported by the Defect Engineered Metal Organic Framework HKUST 1 and Applied in the Aerobic Oxidation of Cinnamyl Alcohol. *Catal. Sci. Technol.* **2019**, *9*, 3703−3710.

(56) Fan, Z. Y.; Wang, J. J.; Wang, W. J.; Burger, S.; Wang, Z.; Wang, Y.; Wöll, C.; Cokoja, M.; Fischer, R. A. Defect Engineering of Copper Paddlewheel Based Metal Organic Frameworks of Type Nott 100: Implementing Truncated Linkers and Its Effect on Catalytic Properties. *ACS Appl. Mater. Interfaces* **2020**, *12*, 37993−38002.

(57) Heinz, W. R.; Agirrezabal Telleria, I.; Junk, R.; Berger, J.; Wang, J.; Sharapa, D. I.; Gil Calvo, M.; Luz, I.; Soukri, M.; Studt, F.; et al. Thermal Defect Engineering of Precious Group Metal−Organic Frameworks: A Case Study on Ru/Rh HKUST 1 Analogues. *ACS Appl. Mater. Interfaces* **2020**, *12*, 40635−40647.

(58) Wang, W. J.; Sharapa, D. I.; Chandresh, A.; Nefedov, A.; Heissler, S.; Heinke, L.; Studt, F.; Wang, Y.; Wöll, C. Interplay of Electronic and Steric Effects to Yield Low Temperature CO Oxidation at Metal Single Sites in Defect Engineered HKUST 1. *Angew. Chem., Int. Ed.* **2020**, *59*, 10514−10518.

(59) Wang, Y.; Wöll, C. IR Spectroscopic Investigations of Chemical and Photochemical Reactions on Metal Oxides: Bridging the Materials Gap. *Chem. Soc. Rev.* **2017**, *46*, 1875−1932.

(60) Yang, C.; Yu, X.; Heißler, S.; Nefedov, A.; Colussi, S.; Llorca, J.; Trovarelli, A.; Wang, Y.; Wöll, C. Surface Faceting and Reconstruc tion of Ceria Nanoparticles. *Angew. Chem., Int. Ed.* **2017**, *56*, 375−379.

(61) Chen, A.; Yu, X.; Zhou, Y.; Miao, S.; Li, Y.; Kuld, S.; Sehested, J.; Liu, J.; Aoki, T.; Hong, S.; et al. Structure of the Catalytically Active Copper−Ceria Interfacial Perimeter. *Nat. Catal.* **2019**, *2*, 334−341.

(62) Wöll, C. Structure and Chemical Properties of Oxide Nanoparticles Determined by Surface Ligand IR Spectroscopy. *ACS Catal.* **2020**, *10*, 168−176.

(63) Yang, C.; Capdevila Cortada, M.; Dong, C.; Zhou, Y.; Wang, J.; Yu, X.; Nefedov, A.; Heißler, S.; López, N.; Shen, W.; et al. Surface Refaceting Mechanism on Cubic Ceria. *J. Phys. Chem. Lett.* **2020**, *11*, 7925−7931.

(64) Lin, X.; Jia, J.; Zhao, X.; Thomas, K. M.; Blake, A. J.; Walker, G. S.; Champness, N. R.; Hubberstey, P.; Schröder, M. High H_2 Adsorption by Coordination Framework Materials. *Angew. Chem., Int. Ed.* **2006**, *45*, 7358−7364.

(65) Wang, Y.; Glenz, A.; Muhler, M.; Wöll, C. A New Dual Purpose Ultrahigh Vacuum Infrared Spectroscopy Apparatus Optimized for Grazing Incidence Reflection as Well as for Transmission Geometries. *Rev. Sci. Instrum.* **2009**, *80*, No. 113108.

(66) Reva, I. D.; Plokhotnichenko, A. M.; Radchenko, E. D.; Sheina, G. G.; Blagoi, Y. P. The IR Spectrum of Formic Acid in an Argon Matrix. *Spectroc. Acta, Part A: Mol. Biomol. Spectrosc.* **1994**, *50*, 1107−1111.

(67) Davies, J. A.; Besley, N. A.; Yang, S.; Ellis, A. M. Probing Elusive Cations: Infrared Spectroscopy of Protonated Acetic Acid. *J. Phys. Chem. Lett.* **2019**, *10*, 2108−2112.

(68) Jiang, J. C.; Yaghi, O. M. Brønsted Acidity in Metal Organic Frameworks. *Chem. Rev.* **2015**, *115*, 6966−6997.

(69) Hadjiivanov, K. I.; Vayssilov, G. N. Characterization of Oxide Surfaces and Zeolites by Carbon Monoxide as an IR Probe Molecule. *Adv. Catal.* **2002**, *47*, 307−511.

(70) Vimont, A.; Goupil, J. M.; Lavalley, J. C.; Daturi, M.; Surblé, S.; Serre, C.; Millange, F.; Férey, G.; Audebrand, N. Investigation of Acid Sites in a Zeotypic Giant Pores Chromium (III) Carboxylate. *J. Am. Chem. Soc.* **2006**, *128*, 3218−3227.

Repository KITopen

Dies ist ein Postprint/begutachtetes Manuskript.

Empfohlene Zitierung:

Wang, J.; Wang, W.; Fan, Z.; Chen, S.; Nefedov, A.; Heißler, S.; Fischer, R. A.; Wöll, C.; Wang, Y.
Defect-engineered metal − Organic frameworks: A thorough characterization of active sites using CO as a probe molecule
2021. The journal of physical chemistry <Washington, DC> / C, 125
doi: 10.554/IR/1000129355

Zitierung der Originalveröffentlichung:

Wang, J.; Wang, W.; Fan, Z.; Chen, S.; Nefedov, A.; Heißler, S.; Fischer, R. A.; Wöll, C.; Wang, Y.
Defect-engineered metal − Organic frameworks: A thorough characterization of active sites using CO as a probe molecule
2021. The journal of physical chemistry <Washington, DC> / C, 125 (1), 593–601.
doi:10.1021/acs.jpcc.0c09738